Dalton Transactions

Accepted Manuscript

ROYAL SOCIETY OF CHEMISTRY

www.rsc.org/dalton

Dalton Transactions

Dynamic Article Links ►

Cite this: DOI: 10.1039/c0xx00000x

www.rsc.org/xxxxxx

ARTICLE TYPE

Structural Transformation of $Bi_{1-X/3}V_{1-X}Mo_XO_4$ Solid Solutions for Light-Driven Water Oxidation

Katerina V.Terebilenko,*[a] Konstantin L. Bychkov[a], Vyacheslav N. Baumer[b],Nikolay S. Slobodyanik[a], Mariia V. Pavliuk[a,c], Anders Thapper[c], Inna I. Tokmenko[d], Iurii M. Nasieka[e], Viktor V.Strelchuk[e]

Received (in XXX, XXX) Xth XXXXXXXXX 20XX, Accepted Xth XXXXXXXXX 20XX
DOI: 10.1039/b000000x

The influence of molybdenum content for solid solutions $Bi_{1-x/3}V_{1-x}Mo_xO_4$ (x = 0.05 – 0.20) on morphology, band gap, structure and light-driven water oxidation properties have been studied by scanning electron microscopy, X-ray powder diffraction and vibrational spectroscopy (Raman and infrared). To find out the peculiarities of structural changes for bismuth scheelite-related oxides containing both vanadium and molybdenum crystal of $Bi_{0.98}V_{0.93}Mo_{0.07}O_4$ have been grown from K – Bi – V – Mo – O high-temperature melt and characterized by single crystal X-Ray diffraction. For the scheelite-related framework both V and Mo were found to occupy the same position lowering the point group symmetry of tetrahedra from 4/m to 2/m giving monoclinic distortion for solid solutions with x = 0.05 – 0.10. The most promising photocatalytic performance was obtained for $Bi_{0.96}Mo_{0.10}V_{0.90}O_4$, of which the oxygen evolution could reach 21μM in 50 s under visible light of LEDs, λ = 470 ± 10 nm, 820 μE cm^{-2} s^{-1}. The changes in catalytic properties are shown to be governed by crystal structure strain with maximum obtained for the boundary sample between monoclinic and tetragonal phase.

Introduction

Over the last decade, the search for novel heterogeneous water oxidation catalysts has been focused on semiconductors with small band gap values to increase the solar energy utilization efficiency[1-3]. Among oxide compounds the derivatives of bismuth vanadate have attracted considerable attention due to high framework flexibility to phase transitions and toward different substitutions[3] that lead to band gap change, high stability, and low cost[2,4]. Being one of the most promising candidates to cover the major demands for heterogeneous water oxidation, $BiVO_4$ suffers from some disadvantages mainly connected with poor photo induced electron transportation, slow kinetics for oxygen evolution and the presence of uncontrolled defects[5]. To overcome the above mentioned difficulties, the main sources of complexity such as spontaneous phase transformation and the influence of doping should be studied in depth, not only in the light of catalytic performance but also to give the insight to synthesis – structure – property relationships.

From a structural point of view, there are three polymorphs of $BiVO_4$: two tetragonal (scheelile and zircon structural types) and a monoclinic one (distorted scheelite - fergusonite structure)[5]. The type of crystal structure and morphology essentially depend on synthetic procedures, raw materials used and reaction conditions[6-9]. Applying high temperatures is more likely to lead to tetragonal scheelite structure[8] or less commonly to the monoclinic crystallites with an irregular shape and large crystal size as well as defects as a result of rapid quenching[5]. The latter structure is unfavourable for the photocatalytic performance. The thermal relationships between these three polymorphs have already been studied[10]. When tetragonal zircon $BiVO_4$ is heated up to 500 ºC the monoclinic form is obtained, while the phase transformation between monoclinic scheelite and tetragonal scheelite bismuth vanadate occurs reversibly at 255 ºC. It is important to point out, that monoclinic $BiVO_4$ is generally less stable, but it is more favourable for detailed studies regarding photocatalytic activity than the tetragonal ones. The monoclinic $BiVO_4$ also shows greatly improved charge-transfer characteristics and a smaller band gap of 2.34 eV[11].

One of the ways of stabilizing low symmetry $BiVO_4$ is doping by transition or rare-earth metals within the cationic or anionic sublattice. For example, partial substitution of Bi^{3+} with Eu^{3+}, Sm^{3+}, or Nd^{3+} leads to tetragonal[12,13] or a mixture of monoclinic and tetragonal phases[14,15].

Generally, bismuth vanadate with scheelite-related structure exhibits significant compositional flexibility toward different substitutions including isovalent and aliovalent ones within cationic and anionic sublattice. Although the isovalent approach has been widely explored for both types of substitution giving a

set of novel solid solutions (fig.1), the cosubstitution or "chemical unit cosubstitution"[16,17] approach has been shown to be more successful for a case of mixed anionic vanadate-molybdate sublattice. Since there is a difference in charges for VO_4^{3-} and MoO_4^{2-} species, the addition of uni-[18] or divalent[19] metal is applied.

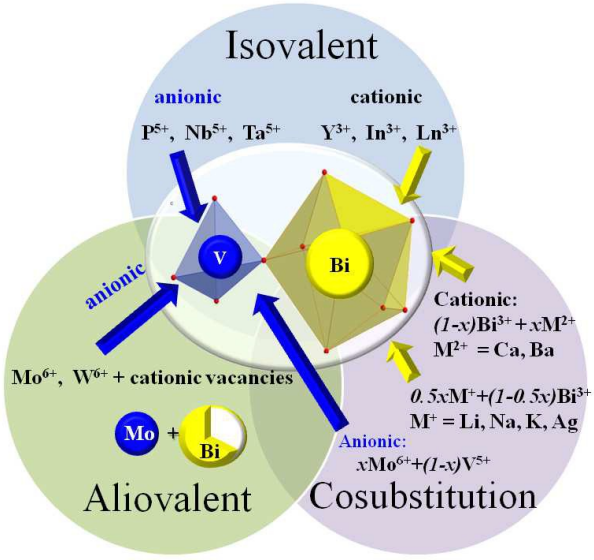

Fig.1. The structural diversity within scheelite-relared framework based on $BiVO_4$ achieved by isovalent, aliovalent and cosubstitution approach

The aliovalent substitution in the anionic sublattice is reported to be more successful for monoclinic structure stabilization. This has been shown for solid solutions of $BiV_{1-x}Nb_xO_4$[6] for the range of x = 0.050 – 0.075 and for the more known examples of Mo:$BiVO_4$[20] and W:$BiVO_4$[21]. The latter compound has showed much improved activity for water oxidation which has been explained by high acidity on the surface compared to pure $BiVO_4$. Recently a more efficient photoelectrode[21] based on anion-substituted $BiVO_4$ has been developed with carrier-separation efficiencies of up to 80% showing that this type of material could be used in practical applications in the future[21].

Unfortunately, the theoretical and synthetic background in this area is far from being clear. Questions about the peculiarities of Mo^{6+} - V^{5+} substitution in the tetrahedral site, the influence of the doping agent concentration on structure, defects formation and water oxidation catalysis are still unanswered. The first data on $Bi_{1-X/3}V_{1-X}Mo_XO_4$ solids formation prepared by a solid state technique have shown a narrow window for solid solutions formation up to x = 0.2 due to the presence of an admixture of Bi_2MoO_6 with higher x value. Moreover, the solids have been indexed in the tetragonal system[22]. Recently, Zhou *et al.* have reported for a ferroelastic phase transition from monoclinic to tetragonal after x = 0.1 without admixtures for the same system[23]. Herein, the investigation of solid solutions of $Bi_{1-X/3}V_{1-X}Mo_XO_4$ (x = 0.05 – 0.20) formation is focused on synthesis -structure-activity relationships in order to clarify the influence of Mo incorporation on structure and catalytic activity. The key features of structure change provoked by the Mo content are studied based on single crystal data and Rietveld analysis for powdered samples.

Experimental

Synthesis

To prepare single crystals of $BiVO_4$ doped with molybdenum the molten system K – Bi – Mo – V – O has been briefly studied. The composition of molten salts corresponds to a KVO_3-$K_2Mo_2O_7$-$BiVO_4$ mixture with molar ratio 8:2:1, where $K_2Mo_2O_7$ plays the role of the flux and the doping agent. Experiments were carried out using analytically pure K_2CO_3, $(NH_4)_6Mo_7O_{24}$, KVO_3 and Bi_2O_3. At the first step $K_2Mo_2O_7$ has been prepared by melting a mixture of K_2CO_3 and $(NH_4)_6Mo_7O_{24}$ at 550°C followed by annealing for 1h to form potassium dimolybdate. Calculated amount of the reagents were preheated at 700°C and were held at 900 °C during 2-3 hours in a platinum crucible in the air. A homogeneous high-temperature solution obtained in this way was gradually cooled with a rate of 100°C /h to 500°C and, finally, poured out on a copper sheet. Crystalline products were retrieved from a solidified melt in hot distilled water.

Solid solutions of $Bi_{1-X/3}V_{1-X}Mo_XO_4$ (x = 0.05, 0.08, 0.10, 0.15 and 0.20) have been synthesized by conventional solid-state sintering technique. The reagent-grade raw materials were Bi_2O_3, $(NH_4)_6Mo_7O_{24}$ and V_2O_5 powders with purity of more than 99.9 %. Stoichiometric amounts of the reagents have been thoroughly mixed with an agate mortar and pestle into fine powders. The samples were gradually heated to 500 °C for 8 h, 600 °C for 8 h, 700 °C for 8 h, and 750 °C for 40 h in alumina crucibles with intermediate regrinding.

Chemical Composition

ICP-AES determination of K, Bi, Mo, and V was performed on a ''Spectroflame Modula ICP'' (''Spectro'', Germany) instrument. Elemental analysis of the single crystals obtained from the melt shows that Bi/V/Mo ratio is 0.98/0.93/0.07, which was used for structural analysis. FTIR spectra were collected at room temperature in KBr disks using a Perkin Elmer Spectrum BX FTIR spectrometer at 400−4000 cm^{-1}. Raman spectrum of a single crystal $BiVO_4$:Mo has been recorded on Horiba Jobin Yvon Scientific XploRa confocal micro-Raman spectrometer under excitation of a green laser at 532 nm. Raman spectra of solid solutions have been recorded on Horiba Jobin-Yvon T64000 under excitation at 514 nm. SEM images have been obtained on JEOL JSM 6060 LV on powders coated with gold. Diffuse reflectance spectra were collected at room temperature using Thermo Scientific Evolution 600 UV-Vis spectrometer equipped with R-928 red sensitive photomultiplier tube. The spectra were recorded in the range of 190-600 nm with 0.2 nm resolution.

X-ray crystallography

The X-ray diffraction patterns were collected using a conventional powder diffractometer Siemens D500 operating in Bragg–Brentano (θ/2θ) geometry using Ni β-filtered, CuKα radiation. The crystal structures of powders were refined with the Rietveld method[24] using the FULLPROF software[25](Table 1). For a single crystal $Bi_{0.98}V_{0.93}Mo_{0.07}VO_4$ diffraction data were collected on an Oxford Diffraction XCalibur-3 diffractometer equipped with a 4 MPixel CCD detector using monochromatized Mo Kα radiation (λ = 0.71073 Å). The structure was solved using direct methods by SHELXS-97 and refined in the full-matrix

least-squares technique in the anisotropic approximation using the SHELXL-97[26] program packages (Table 2). The Mo/V ratio was constricted according to the chemical analysis.

Oxygen evolution experiments

The procedure used was the same as reported earlier by Kurz et al[27]. The signal of a standard Clark electrode (Hansatech Instruments), separated from the sample solution by a Teflon membrane, was recorded for the entire duration of the experiment at 0.1 s intervals using the Oxygraph v1.02 software package by Hansatech Instruments. The cell was placed on top of a magnetic stirrer to continuously stir the solution using a small, Teflon-coated stirrer bar. Air saturated water solutions ([O_2] = 280 μM 21°C) were used for calibration of the electrode. The cell was purged with argon gas (via a tube inserted through a channel in the plunger) before each experiment.

A fresh solution of the powders was prepared in deionized H_2O (100 mL) before each experiment. Standard concentrations of components in the catalytic system in a Clark cell were: 1 mg of a studied compound, 0.2 mM of $[Ru(bpy)_3](ClO_4)_2$, 1 mM of $Na_2S_2O_8$ in 0.04 M borate buffer (pH 8.5). The samples were transferred to the Clark cell and kept thermostated inside the double walled, optically transparent cell at 21 °C and the cell was purged with argon gas (via a tube inserted through a channel in the plunger) before each experiment. The volume of the sample in the cell was 1 mL. After all dissolved oxygen had been removed, visible light LEDs (λ = 470 ± 10 nm, 820 μE cm^{-2} s^{-1}) were used to start the photoreaction.

Table 1. Unit Cell Parameters for $Bi_{1-x/3}V_{1-x}Mo_xO_4$ (0.05≤x≤0.20) solid solutions and BVS values for Bi and V/Mo polyhedra

Compound	Space group	a, Å	b, Å	c, Å	β	Density	V , Å^3	R (Bragg, %)	BVS(Bi)	BVS (V/Mo)	Average apparent size and standard deviation (anisotropy)(Å^3)
$Bi_{0.98}Mo_{0.05}V_{0.95}O_4$	I2/a	5.10666(9)	11.69286(19)	5.18300(9)	90.2540(15)	6.94	309.482(9)	4.23	3.02	4.91	1074.89 (2.37)
$Bi_{0.97}Mo_{0.08}V_{0.92}O_4$	I2/a	5.10712(12)	11.6909(2)	5.18138(11)	90.2545(18)	6.86	309.361(12)	5.87	2.99	4.84	1050.83 (1.58)
$Bi_{0.96}Mo_{0.10}V_{0.90}O_4$	I2/a	5.113801(16)	11.69046(3)	5.178411(15)	90.2006(3)	6.83	309.5774(16)	6.58	3.07	4.78	1099.58 (2.45)
$Bi_{0.95}Mo_{0.15}V_{0.85}O_4$	$I4_1/a$	5.15673(10)	-	11.69131(19)	90	6.80	310.894(10)	3.68	2.80	5.22	1057.98 (1.62)
$Bi_{0.93}Mo_{0.20}V_{0.80}O_4$	$I4_1/a$	5.16509(9)	-	11.6901(2)	90	6.74	311.869(10)	3.61	2.73	5.46	1082.67(1.84)

Results and discussion

The crystal structure of $Bi_{0.98}V_{0.93}Mo_{0.07}O_4$ is best described as a defect scheelite one. The Bi and Mo/V atoms are found at the specific positions with partial site distribution, while four O atoms are located at the general 8f position being fully occupied (Table 3). There is one unique Bi site at the Wyckoff position 4e showing a coordination of eight oxygen atoms in a shape of distorted square antiprism with occupancy of 0.98 (Fig.2).

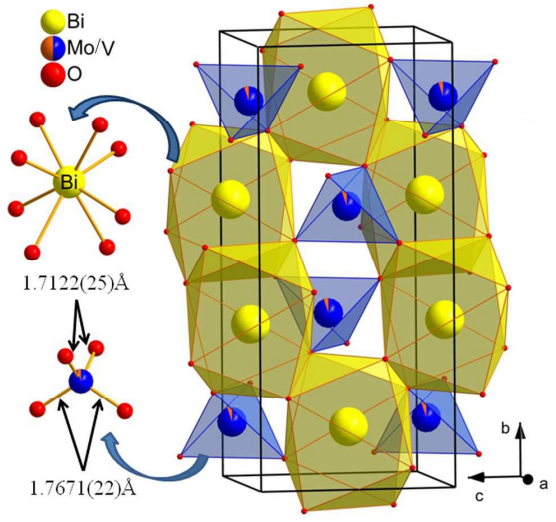

Fig.2. The crystal structure of $Bi_{0.98}V_{0.93}Mo_{0.07}O_4$ showing mixed (Mo,V)O_4 tetrahedron.

The Bi-O distances range from 2.3788(10) to 2.5992(22)Å and are close to those found for isotopic compounds (Table 4). Both V and Mo atoms are situated at the same Wyckoff position 4e with occupancy of Mo equal to 0.07. They are tetrahedrally surrounded by oxygen atoms and (Mo/V)-O distances are 1.712(3)×2 and 1.767(2)×2 Å having 2-fold symmetry.

The charge compensation of aliovalent substitution V^{5+} by Mo^{6+} is realized by the presence of Bi^{3+} vacancies in the structure. As a result, a monoclinic distortion of the parent scheetile structure occurs with a formula $Bi_{2/3}\square_{1/3}V_{0.93}Mo_{0.07}O_4$.

It is important to compare both the $BiVO_4$ tetragonal structure and the monoclinic one doped with molybdenum. The flexibility of the scheelite structural motif with symmetry decrease is achieved by local polyhedral distortion for Bi and Mo/V ions.

Table 2. Details of single-crystal data collection, structure solution and refinement for $Bi_{0.98}V_{0.93}Mo_{0.07}O_4$

Formula weight	320.93
Space group	I 2/a
Formula units, Z	4
a/Å	5.1153(3)
b/Å	11.7022(5)
c/Å	5.1878(2)
β/°	90.244(5)
Volume/Å^3	310.54(3)
X-ray density/g cm^{-3}	6.864
Range θmin–θmax	3.48 - 66.32
Range h; k; l	$-13 \le h \le 13, -14 \le k \le 29, -13 \le l \le 13$
R_{all}	0.0712
Gof	0.994

The bond distances V-O in the tetragonal structure are equal, while there are two types of them in case of monoclinic one.

Table 3. Atomic coordinates for $Bi_{0.98}V_{0.93}Mo_{0.07}O_4$

Atom	Wyck.	occ.	x/a	y/b	z/c
Bi1	4e	0.97662	1/4	0.63158(1)	0
Mo1	4e	0.07022	-1/4	0.62936(4)	1/2
V1	4e	0.92976	-1/4	0.62936(4)	1/2
O1	8f	1	0.0078(5)	0.70729(18)	0.6443(4)
O2	8f	1	-0.1160(5)	0.55018(19)	0.2565(5)

Interestingly, the compound obtained takes an intermediate place between the tetragonal scheelite $BiVO_4$ where Bi^{3+} positions are fully occupied and $Bi_2(MoO_4)_3$, where the ordered arrangement of vacancies (□) gives a $Bi_{2/3}□_{1/3}MoO_4$ structure[28].

Table 4. Selected interatomic distances (Å), angles (°)

BiO_8 polyhedra	$(V,Mo)O_4$ tetrahedra	
Bi-O, Å	(Mo,V)-O, Å	<O-(Mo,V)-O,°
2×2.3788(22)	2×1.7671(24)	2×106.945(106)
2×2.3886(22)	2×1.7122(25)	2×105.493(106)
2×2.4909(25)		117.862(110)
2×2.5994(24)		114.473(121)

Generally, IR spectroscopy for this type of compounds gives little information due to the broadening of the stretching bands in the range of 550-900 cm^{-1}, especially in the case of crystallographic sharing of anionic groups by different atoms. On the contrary, Raman spectrum is quite informative. The room temperature Raman and IR spectra of $Bi_{0.98}V_{0.93}Mo_{0.07}O_4$ are displayed in Fig.3. On the basis of known trends of positions and relative intensities of the Raman bands for VO_4 and MoO_4 tetrahedra the most strong band centered at 824 cm^{-1} is assigned to $\nu_s(V\text{-}O)$, while the weak shoulder at about 713 cm^{-1} to $\nu_{as}(V\text{-}O)$ respectively.

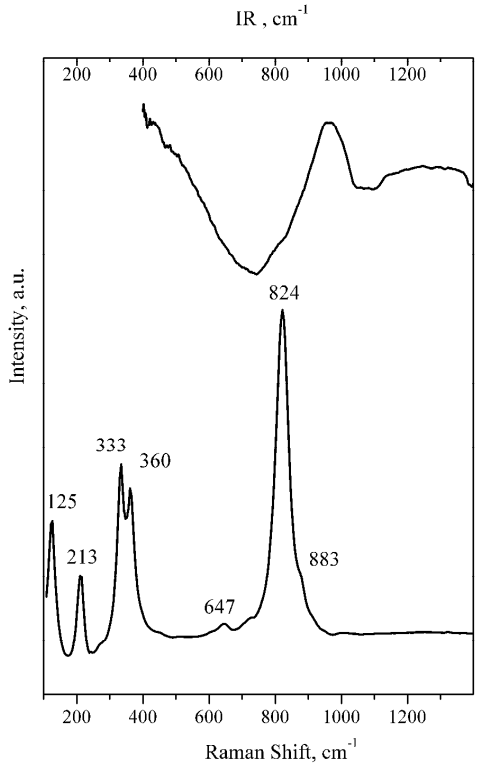

Fig.3 IR and Raman Spectra of $Bi_{0.98}V_{0.93}Mo_{0.07}O_4$ single crystal

The impact of MoO_4 stretching vibrations may be seen due to a presence of a shoulder near 883 cm^{-1}. The bending modes $\delta_s(VO_4)$ and $\delta_{as}(VO_4)$ are at 360 and 333 cm^{-1}, respectively, and external modes (rotation/translation) occur at 213 and 125 cm^{-1}. Splitting of bending modes in the region of 360-325 cm^{-1} is believed to be a spectroscopic feature of the monoclinic phase[22].

The results of single crystal structure solving and spectroscopic characteristics of $Bi_{0.98}V_{0.93}Mo_{0.07}O_4$ have been used for comparison of ceramics obtained by solid state synthesis.

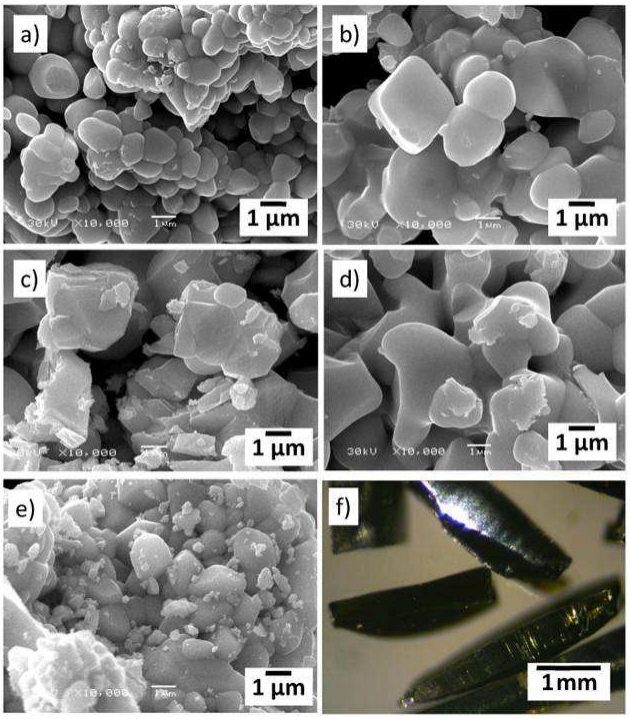

Fig.4. SEM images of $Bi_{1-x/3}V_{1-x}Mo_xO_4$, where x = 0.05(a), 0.08(b), 0.10(c), 0.15(d), 0.20(e) and an image of $Bi_{0.98}V_{0.93}Mo_{0.07}O_4$ single crystal (f)

Due to the application of different synthetic pathways, the shape and the size of the particles differ significantly. The SEM micrographs of solid solutions $Bi_{1-x/3}V_{1-x}Mo_xO_4$ (x = 0.05, 0.08, 0.10, 0.15, 0.20) is presented on Fig. 4. The product crystallizes in a compact form with an average size of about 1–3 µm (Fig. 4a). The particles are well separated and a grain boundary between the microcrystals is clearly seen. The spherical-like shaped particles develop loose agglomerates. With an increase of the Mo^{6+} up to 15 mol % (Fig. 4c, d), the particles are glued together to form bigger aggregates with wider size distribution. At the highest molybdenum content studied (Fig.4e) the sample exhibits lots of non-dispersed particles with quite irregular shape. On the contrary, the single crystals $Bi_{0.98}V_{0.93}Mo_{0.07}O_4$ obtained from molten salts are found to crystallize in a shape of dark needles (Fig. 4f).

The XRD patterns of $Bi_{1-x/3}V_{1-x}Mo_xO_4$ (x = 0.05, 0.08, 0.10, 0.15, 0.20) solid solutions are displayed in Fig. 5. The maximum content of molybdenum as a doping agent in $BiVO_4$ host for catalytic performance previously has been estimated as equal to 2 mol %[20]. All of the samples with different molybdenum content present similar scheelite-related diffraction patterns without impurity peaks. It is well-known that the difference in the XRD patterns between monoclinic and tetragonal ones can be distinguished by the splitting of peaks at 18.5°, 35°, and 46° of 2θ[23], which are observed for x = 0.05, 0.08, and 0.10. As a result,

the first three points (0.05-0.10) are indexed in the monoclinic system (JCPDS No. 14–0688), while the solids containing x = 0.15 and 0.20 of molybdenum is described in the tetragonal symmetry (JCPDS No. 14–0133).

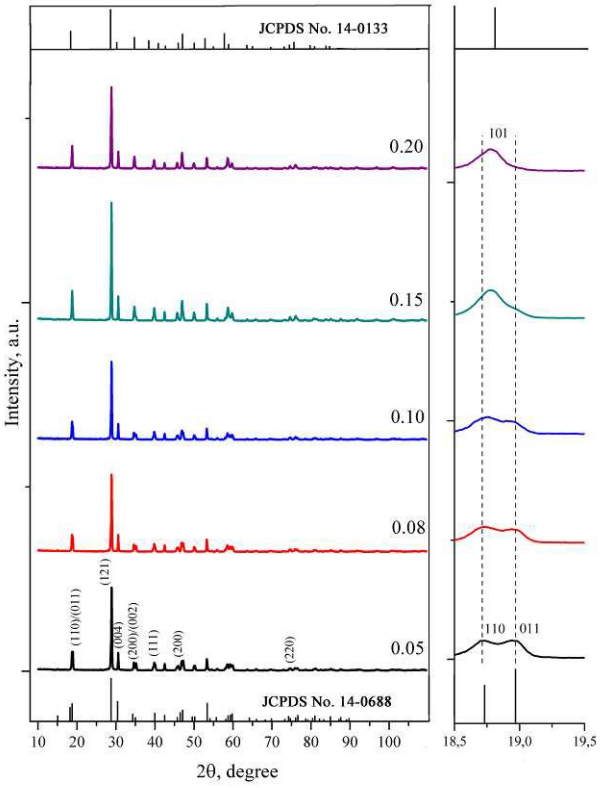

Fig.5. XRD patterns of the $Bi_{1-X/3}V_{1-X}Mo_XO_4$ ($0.05 \le x \le 0.20$) samples and the magnified view of the (110)and (011) diffraction peaks as a function of *x*.

The literature data concerning the boundary value of *x* between monoclinic and tetragonal systems differ significantly. Thus, in case of the hydrothermal reaction the mixture of them are observed for x =0.4-0.75[29], while for solid state synthesis the monoclinic distortion has been found to be near $x = 0.75$[30] or $x = 0.1$[23]. Herein, the data obtained are in agreement with Zhou *et. al.*[23] having the boundary value of $x = 0.1$. Consequently, the progressive doping of Mo^{6+} has complex influence on structure: small amounts (0.05–0.10) of the Mo^{6+} admixture provokes a symmetry decrease toward the *I2/a* space group, while higher amounts of Mo (15 % and more[23]) gives tetragonal symmetry again.

The atomic coordinates of single crystal data for $Bi_{0.98}V_{0.93}Mo_{0.07}O_4$ were used to determine the structure of the series of solid solutions $Bi_{1-X/3}V_{1-X}Mo_XO_4$ (x = 0.05, 0.08, 0.10, 0.15, 0.20). The concentration of Mo was constrained in accordance to nominal compositions. All of the metal atoms were refined using isotropic thermal parameters. The refinement was stable and gave low R-factors. The main refinement parameters are summarized in Table 4.

The Fig. 6 (a) shows the variations of cell parameters *a*, *c*, cell volume and crystallographic density. As the molybdenum content increases, the cell parameter *a* smoothly increases, while *c* parameter decreases up to the point x = 0.1, where both parameters merge into one indicating the crystal structure change form monoclinic to tetragonal. The value of monoclinic angle β decreases with the increase of x and remains close to 90° (Table 1), which is reflected in the XRD patterns by merging of (110) and (011) into one peak (101).The experimental (dots) and theoretical (lines) X-ray diffraction patterns of the samples are given for $Bi_{0.98}V_{0.95}Mo_{0.05}O_4$ in fig 6b and for others in Fig. 1S–4S.

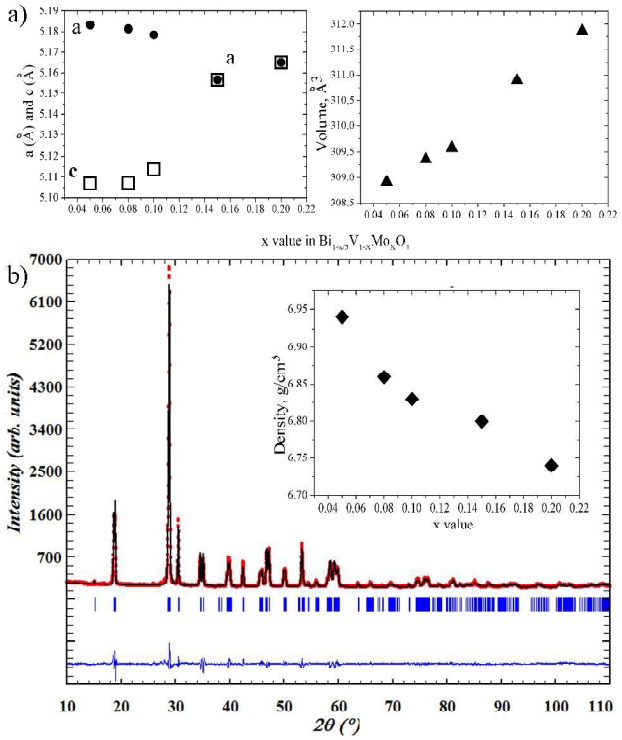

Fig. 6. The dependence of the *a*, *c* parameters and cell volume on *x* (a); the experimental and calculated XRD patterns, Rietveld difference plot of $Bi_{0.98}V_{0.95}Mo_{0.05}O_4$ (b). The inset shows crystallographic density change for $Bi_{1-X/3}V_{1-X}Mo_XO_4$

Based on the Rietveld refinement results, the unit cell volume is proportional to *x*, which also confirms that the solutions belong to the same crystal structure family. On the other hand, the density of each solid solution slightly decreases with the increase of Mo content. This fact confirms partial occupancy of cationic positions by Bi^{3+} in the scheelite structure and presence of vacancies in the framework. Thus, it can be concluded that the increase of volume in $Bi_{1-X/3}V_{1-X}Mo_XO_4$ solid solutions is caused predominantly by unit cell elongation parallel to the *a*-axis.

To study the stability of the mixed framework obtained in comparison with the parent one the bond-valence sums (BVSs) were calculated using parameters from[31]. For partially occupied sites the equation:

$$S = \exp((Ro-R)/0.37)$$

was modified including R_o parameter for substituted position[32]:

$$R_0 = R_0(V)\times Oc(V) + R_0(Mo)\times Oc(Mo)$$

where $R_0(V)$ and $R_0(Mo)$ are bond-valence parameters and Oc(V) and Oc(Mo) – the crystallographic occupancies. The mean-calculated BVS value for V/Mo positions for solid solutions are increasing with Mo content (Table 1), that is expected for tetraherally coordinated mixed sites taking into account linear

sum of V-O and Mo-O distances with corresponding occupancies.

The BVS values for Bi sites are in good agreement with expected value for x = 0.05-0.15, while for a higher Mo content the Bi position seems to be slightly unbonded (Table 1), that is connected with the influence of vacancies formation.

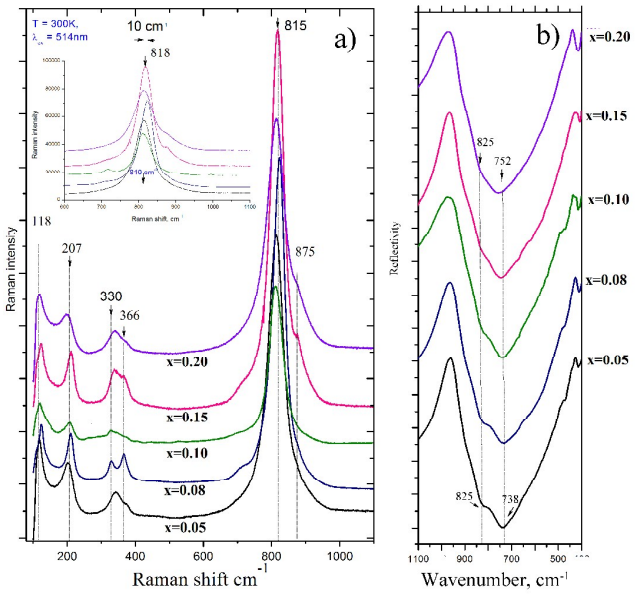

Fig. 7. Raman (a) and FTIR (b) spectra for $Bi_{1-X/3}V_{1-X}Mo_XO_4$

One of the most important crystal-chemical questions arises due to a specific change in scheelite symmetry while doping at the anionic sublattice. While doping with molybdenum the symmetry of the framework is lowered to monoclinic one but strictly by the value x = 0.1. This limitation is common for the majority of scheelite-related compounds containing both vanadate and molybdate groups.

Thus, for solid solutions $(M_{0.5x}Bi_{1-0.5X})(Mo_xV_{1-x})O_4$, where M = Li, Na, K)[33-35] the phase boundaries are given in Table 5 as well as their Raman bands positions. Importantly, that the monoclinic to tetragonal structural change is believed to be followed by shift of the bands in the region near 820 cm^{-1} , while two bands in the area of 320-370 cm^{-1} are expected to merge into one[33].In case of solids prepared the phase change is also observed at x =0.1, but the Raman bands positions and their shift differs (Fig. 7). Thus, there are two trends for the band blueshifting near 815 cm^{-1}. The most intensive band in the Raman spectra of the compounds studied is ascribed to $v_s(V\text{-}O)$. The blueshifting of this band with the increase of x differs for x = 0.05- 0.1 (monoclinic) and x =0.15, 0.20 (tetragonal). The same situation occurs in case of two bands at 330 and 366 cm^{-1} corresponding to bending modes $\delta_s(VO_4)$ and $\delta_{as}(VO_4)$, respectively. They do not merge, but their intensities redistributes with increase in x as it was shown for Ca and Bi containing scheelites[35].

On the contrary, IR spectra for solid solutions studied agree well with literature data possessing one broad band and a shoulder in the range 550-900 cm^{-1} which smoothly shifts toward higher wave numbers due to a substitution of V^{5+} by the heavier Mo^{6+}.

Table 5. The solid solutions with scheelite-related structure with Raman shift corresponding to mixed $(V/Mo)O_4$ tetrahedra

Solid solution	Structure boundaries	$v_s(V\text{-}O)$	$v_{as}(V\text{-}O)$	$v_{as}(Mo\text{-}O)$	$\delta_s(VO_4)$ and $\delta_{as}(VO_4)$	External modes	Ref.
$(K_{0.5x}Bi_{1-0.5X})(Mo_xV_{1-x})O_4$	$0 \le x \le 0.10$ monoclinic	825.9	714.6	876	367.8 326.3	211.1 128.8	23
	$0.15 \le x \le 0.64$ tetragonal	814		876	344		
$(Li_{0.5}Bi_{0.5})_XBi_{1-X}(Mo_xV_{1-x})O_4$	$0 \le x \le 0.098$ monoclinic	825.9	714.6	872.3	367.8 326.3	211.1 128.2	33
	$0.1 < x \le 1.0$ tetragonal	815.1	772.4	872.3	367.8 326.3	200.6	
$(Na_{0.5x}Bi_{1-0.5X})(Mo_xV_{1-x})O_4$	$0 \le x \le 0.1$ monoclinic	825.8	714.6	870.1	367.8 326.3	211.1 128.2	34
	$0.1 < x \le 1.0$ tetragonal	816.2				211	
$Ca_{1-X}Bi_X(Mo_XV_{1-X})O_4$	$0.1 < x \le 1.0$ tetragonal	815		882	375 340	211	35
$xBi_{2/3}MoO_4$-(1-X)$BiVO_4$	$0 \le x \le 0.1$ monoclinic	825.4	713.6	876.3	366.8 325.3	211.9 127.2	18
	$0.1 < x \le 1.0$ tetragonal	814			340.2		
$Bi_{1-X/3}V_{1-X}Mo_XO_4$	$0 \le x \le 0.1$ monoclinic	815		875	366 330	207 118	this work
	$0.15 < x \le 0.2$ tetragonal	818		875	366 330	207 118	

The $BiVO_4$ was found to be a direct band gap semiconductor capable to act as water oxidation catalyst under visible light illumination. Previously the incorporation of molybdenum into bismuth vanadate has been shown to bring minor changes in the optical absorbance spectra[36]. The absorption spectra of the $Bi_{1-X/3}V_{1-X}Mo_XO_4$ (x = 0.05, 0.08, 0.10, 0.15, 0.20) agree well with literature data[26]. The optical band gap E_g of a semiconductors studied were deduced according to the Kubelka-Munk equation.

The estimated band gaps from the diffusive reflectance spectra are found to be 2.25 eV for all samples (Fig.8).

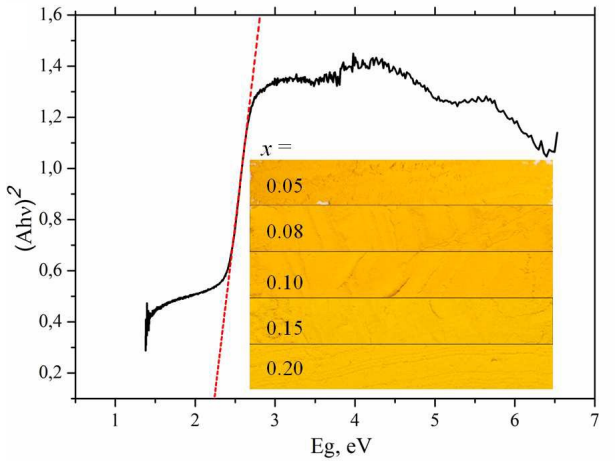

Fig. 8 The band gap estimation for $Bi_{0.96}Mo_{0.10}V_{0.90}O_4$. Inset shows color of the samples.

The unique position of $BiVO_4$ among other oxides in that its valence band is comprised of a coupling between the Bi 6*s* and O 2*p* orbitals which provides destabilization and forces the valence band upward. Conversely, the conduction band includes a coupling between the V 3*d*, O 2*p*, and Bi 6*p*, which lowers the band[36]. This coupling result in a direct band gap semiconductor with a smaller band gap than most oxide compounds and enhanced visible light absorption, leading to its bright yellow color (Fig. 8).

In addition, the coupling of the Bi 6*s* and O 2*p* in the valence band allow for improved hole mobility, which is beneficial for photocatalytic oxidation reactions.

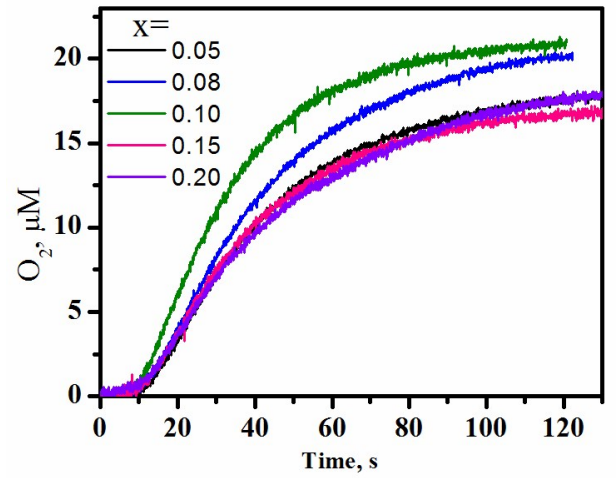

Fig.9. Oxygen evolution traces of the photocatalytic system catalysed by $Bi_{1-x/3}V_{1-x}Mo_xO_4$

When the system was illuminated the O_2 evolution started after a lag-phase of 4–6 s for all studied samples (Fig. 9). The rate of O_2 evolution was almost constant for 30-50 s, after which it decreased. For the five $Bi_{1-X/3}V_{1-X}Mo_XO_4$ (x =0.05, 0.08, 0.10, 0.15, 0.20) samples studied, the amount of produced oxygen was between 18-21 μM. The sample $Bi_{0.96}Mo_{0.10}V_{0.90}O_4$, which produced maximum O_2, and with the highest rate, corresponds to the structural boundary between monoclinic and tetragonal phase. The enhancement in the activity could be due to structural strain in the corresponding solid solution. The increased O_2 evolution observed for x=0.1 is less likely to be related with the surface area due to morphology similarities of the samples (Fig.4) as well as crystallinity or absorption edge. Furthermore, there is a slight difference in photocatalytic activity of the samples which can be due to structural changes induced by the Mo doping.

It is well-known, that monoclinic bismuth vanadate is much more active in water oxidation process than other polymorphs. The doping with 2 % mol. has been shown to stabilize the monoclinic polymorph and to serve as a promising catalyst, but the influence of molybdenum content on catalytic performance as well as structural changes provoked by Mo incorporation has not been studied yet.

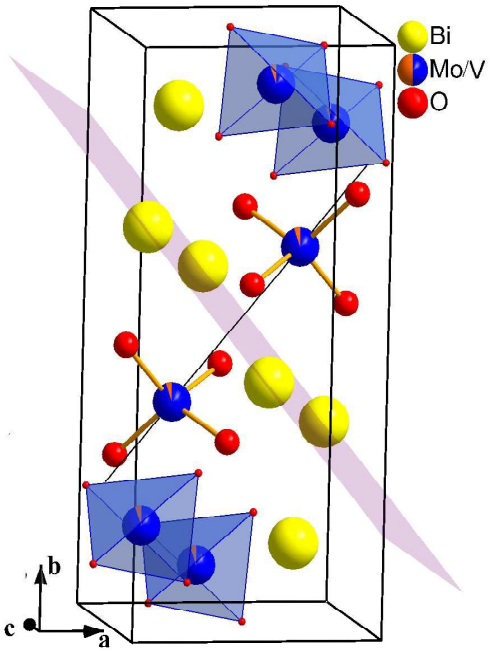

Fig. 10 The unit cell of $Bi_{0.98}V_{0.93}Mo_{0.07}O_4$ showing (1 2 1) plane and a line throughout the mixed Mo/V atoms

Tetragonal and monoclinic scheelite-related $BiVO_4$ have similar framework organization. For both structures the unit cell includes a six-member ring consisting from BiO_8 polyhedra interlinked by common edges showing a chair-like conformation. The four of them are found to lie in the plane (1 2 1) (Fig. 10), while two the nearest tetrahedral species are found above and below this plane. In a light of possible structural reorganization, VO_4 polyhedra in a scheelite structure are more rigid toward distortions than BiO_8 ones. Bi-O bonds are less rigid (more ionic) and should be more sensitive to structural evolution like expansion or compression of corresponding bonds.

In the case of aliovalent substitution in the anionic sublattice the distortion affects both cationic and anionic polyhedra. That means that monoclinic scheelite may be seen as a distorted and compressed version of a scheelite architecture which implies a lowering of the point group symmetry from 4/m to 2/m. The compression may be illustrated by the distance change for the atom above and below the plane (1 2 1). In the tetragonal structure both Bi and V/Mo atoms are equidistant from this plane

at a distance of 1.935(10)Å. Considering the monoclinic structures (x = 0.05, 0.08. 0.10), the distance from Bi atoms to the plane (1 2 1) is shortening to 1.7776(10)Å, while the distance form V/Mo is elongating up to 1.9575(10)Å. Consequently, a line drawn through the two V/Mo atoms intersects the plane (1 2 1) providing an angle near 10º. For tetragonal structures this angle is less than 8º (7.166(1) and 7.068(1)º for x = 0.15 and 0.20 respectively), while for the monoclinic ones it reaches the value of 10º (9.797(8), 9.689(8) and 10.011(1) for x = 0.05, 0.08. 0.10). In addition the (V/Mo)-O distances split for monoclinic compounds, making the $(V,Mo)O_4$ tetrahedra distorted with two short distances (1.7122(25)Å) and two long ones (2.176(24) Å), which bring additional strain to the structure. The Bi and V/Mo atoms shift from the plane as the molybdenum content is increasing to x = 0.1, reaching the x =0.15 means the overall elongation of distances in tetrahedra increasing the symmetry to tetragonal again. The angle discussed may be used as a crystal structure distortion value that impacts the scheelite structure in the way, that the most distorted one corresponds to x = 0.1 as well as the most promising catalytic performance. The crystal structure change here seems to be governed by the $(Mo/V)O_4$ polyhedron distortion, while the boundary solid shows the best catalytic performance in the water oxidation reaction.

Conclusions

The effects of molybdenum incorporation on the crystal structure, morphology, band gap value and photocatalytic activity were investigated by X-ray powder diffraction, scanning electron microscopy, diffusive and vibrational spectroscopy (Raman and infrared). The crystal structure change has been studied in detail for a single crystal $Bi_{0.98}V_{0.93}Mo_{0.07}O_4$ grown from a melt. The best catalytic performance for water oxidation has been found for a sample, $Bi_{0.96}Mo_{0.10}V_{0.90}O_4$, which corresponds to a boundary between tetragonal and monoclinic phase, and have the highest crystal structure strain.

Notes and references

[a] *Department of Chemistry, Taras Shevchenko National University of Kiev, Volodymyrska st, 64/13, 01601, Kiev, Ukraine. Tel: E-mail: tereb@bigmir.net*

[b] *STC "Institute for Single Crystals" NAS of Ukraine, 60 Lenina ave., Kharkiv, 61001, Ukraine*

[c] *National O.O. Bogomoletz Medical University, 13 T. Shevchenko Blvd., Kyiv, Ukraine, 01601*

[d] *Department of Chemistry – Ångström Laboratory, P.O. Box 523, S-75120, Uppsala, Sweden*

[e] *Laboratory of Optical Submicron Spectroscopy, NAS of Science of Ukraine, ,V. Lashkarev Institute of Semiconductor Physics, 45 prosp. Nauki str., 03028, Kiev, Ukraine*

† Electronic Supplementary Information (ESI) available: [details of any supplementary information available should be included here]. See DOI: 10.1039/b000000x/

‡ Footnotes should appear here. These might include comments relevant to but not central to the matter under discussion, limited experimental and spectral data, and crystallographic data.

1. S. Sun and W. Wang, *RSC Adv.*, 2014, **4**, 47136;
2. Z.-F.Huang, L. Pan, J.-J. Zou, X. Zhang and L.i Wang, *Nanoscale*, 2014, **6**, 14044.
3. K.Rajeshwar, A.Thomas and C. Janáky, *J. Phys. Chem. Lett.*, 2015, **6**, 139.
4. D. Zhou, L.-X.Pang, J. Guo, Z.-M. Qi, T. Shao, Q.-P. Wang, H.-D. Xie, X. Yao and C. A. Randall, *Inorg. Chem.*, 2014, **53**, 1048.
5. X. Li, J. Yu, J. Low, Y. Fang, J. Xiao and X. Chen, *J. Mater. Chem. A*, 2015, **3**, 2485.
6. S. S. Fathimah, P. P. Rao, V. James, A.K. V. Raj, G. R. Chitradevi and S. Leela, *Dalton Trans*., 2014, **43**, 15851.
7. A. Walsh, Y. Yan, M. N. Huda, M. M. Al-Jassim, and S.-H. Wei, *Chem. Mater*. 2009, **21**, 547.
8. P. Pookmanee, S. Kojinok and S. Phanichphant, *Journal of Metals, Materials and Minerals*, 2012, **22**,.49.
9. A.W. Sleight, H.-Y. Chen, A. Ferretti and D.E. Cox, *Mat. Res. Bull.,* 1979, **14**, 1571.
10. S. Tokunaga , H. Kato and A. Kudo, *Chem. Mater.*, 2001, **13**, 4624.
11. H. Fan, T. Jiang, H. Li, D. Wang, L. Wang, J. Zhai, D. He, P. Wang and T. Xie, *J. Phys. Chem. C*, 2012, ***116***, 2425.
12. Q.Wang, Y. Li, Z. Zeng and S. Pang, *J. Nanopart. Res.*, 2012, **14**, 1076.
13. Y. Luo, G. Tann, G. Dong, H. Ren and A. Xia, *Ceramics International*, 2015, **41**, 3259.
14. Y. Luo, G. Tan, G. Dong, L. Zhang, J. Huang, W. Yang, C. Zhao and H. Ren, *Applied Surface Science*, 2015, **324**, 505.
15 S. Usai, S. Obregón, A. I. Becerro and G. Colón, *J. Phys. Chem. C,* 2013, **117**, 24479.
16. Z.Xia, C. Ma, M.S.Molokeev, Q.Li, K. Rickert, K.R. Poeppelmeier, *J.Am.Chem.Soc.,* 2015, 12494.
17. J.Zhou, Z. Xia, M.Chen, M. S. Molokeev, Q. Liu, Sci.Rep., 2015, **5**, 12149.
18. D.Zhou, L.-X.Pang, H.Guo, H.Wang, X.Yao, C. Randall, *Inorg. Chem.*, 2011, **50**, 12733-12738.
19. W. Yao and J. Ye, *J. Phys. Chem. B,* 2006, **110**, 11188.
20. W. Yao, H. Iwai and J. Ye**,** *Dalton Trans.*, 2008, 1426–1430.
21. F. F. Abdi, L. Han, A. H. M. Smets, M.Zeman, B. Dam and R. Krol, *Nature Communications,* 2013*,* **4**, 2195.
22. T.Duraisamy, A. Ramanan, *Solid State Ionics*, 1999, **120,** 233-237.
23. D. Zhu, W.-B. Li, L.-X. Pang, J.Guo, Z.-M.Qi, T. Shao, X. Yao, C. Randal, *Dalton Trans., 2014, **43**,* 7290-7297
24. H.M. Rietveld. *J. Appl. Crystallogr.*, 1969, **2**, 65
25. J. Rodriguez-Carvajal, *FULLPROF,* Laboratoire Léon Brillouin (CEA–CNRS), France. 2006.
26. G. M. Sheldrick, *Acta Crystallogr.*2008, **A64**, 112−122
27 P. Kurz, G.Berggren, M.F. Anderlund, S. Styring, *Dalton Trans.,* 2007, 4258.
28 A.F. Elzen, G.D.Rieck, Acta Cryst., 1973, B29, 2433-2436.
29. Z. Zhai, A.B.Getsoian, A.T. Bell, *J.Catalysis*, 2013, **308**, 25-36.
30. D.Zhou, W.G.Qu, C.A. Randal, L.X. Pang, H. Wang, X.G.Wu, J.Guo, G.Q.Zhang, L. Shu, Q.P.Wang, H.C. Liu, X.Yao. Acta Materialia, 2011, **59**, 1502-1509.
31. I. D. Brown, D.Altermatt, *Acta Crystallogr.*1985, **B41**, 244−247.
32. N.S. Slobodyanik, K.V. Terebilenko, I. V. Ogorodnyk, I. V. Zatovsky, M. Seredyuk, V. N. Baumer, P. Gütlich, Inorg.Chem, 2012, **51**, 1380-1385.
33. D.Zhou, L.-X. Pang, H.Wang, J. Gou, X.Yao, C. A. Randall, *J. Mater. Chem. 2011, **21**, 18412-18420.*
34. W. Yao, J. Ye, J. Phys. Chem. B 2006, **110**, 11188-11195
35. Z.F. Huang, L. Pan, J.-J. Zou, X. Zhang, L.Wang., *Nanoscale*, 2014, **6**, 14044–14063.
36. A. Walsh, Y. Yan, M. N. Huda, M. M. Al-Jassim, S-H Wei, *Chem. Mater,* 2009, **21**, 547–551.

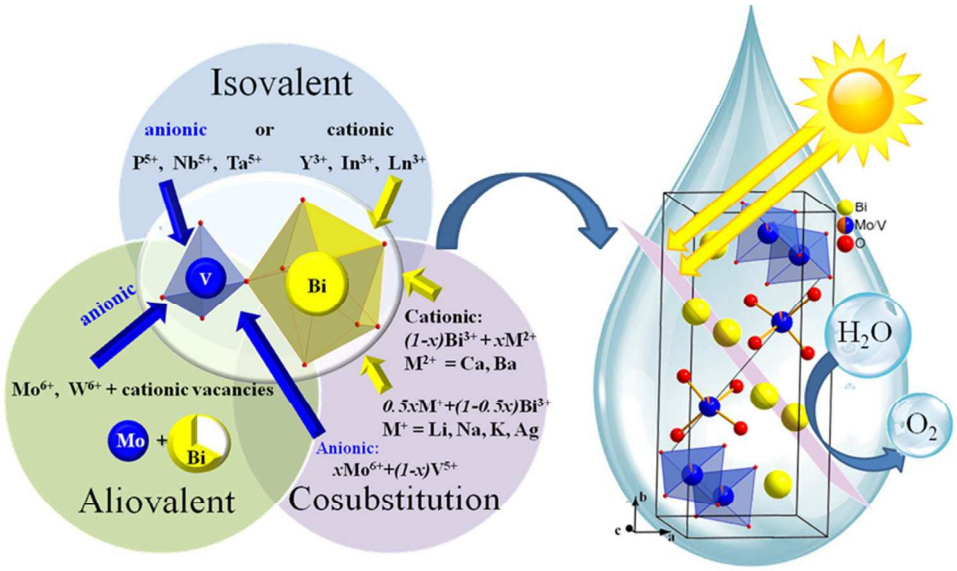

242x144mm (96 x 96 DPI)